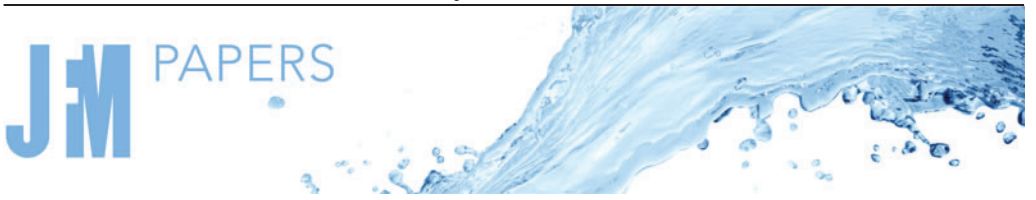
J. Fluid Mech. (2022), *vol*. 949, A17, doi:10.1017/jfm.2022.666



Drop deformation during diffusiophoresis

Brian E. McKenzie[1,2], Henry C.W. Chu[3], Stephen Garoff[2,4], Robert D. Tilton[1,2,5] and Aditya S. Khair[1,2,†]

[1]Department of Chemical Engineering, Carnegie Mellon University, Pittsburgh, PA 15213, USA

[2]Center for Complex Fluids Engineering, Carnegie Mellon University, Pittsburgh, PA 15213, USA

[3]Department of Chemical Engineering, University of Florida, Gainesville, FL 32611, USA

[4]Department of Physics, Carnegie Mellon University, Pittsburgh, PA 15213, USA

[5]Department of Biomedical Engineering, Carnegie Mellon University, Pittsburgh, PA 15213, USA

(Received 17 February 2022; revised 28 June 2022; accepted 27 July 2022)

Diffusiophoresis refers to the motion of a colloidal particle in a solute concentration gradient, animated by particle–solute interactions. We present a theoretical analysis of the diffusiophoretic motion of a viscous drop in a gradient of neutral solute at zero Reynolds number. In a spatially uniform gradient, the translational velocity of a spherical drop was found by Anderson *et al.* (*J. Fluid Mech.*, vol. 117, 1982, pp. 107–121). Here, we show additionally that the drop experiences no tendency to deform, regardless of the magnitude of the interfacial tension at the interface of the drop and suspending fluid. Next, we consider a non-uniform gradient, where the ambient solute concentration takes the form of a quadrupole around the drop centroid. This gradient does not induce drop translation, due to symmetry, but does induce a deformation in the drop shape, which is spheroidal to first order in the capillary number $Ca = \beta k_B T R^2 K/\gamma$, where β is the magnitude of the quadrupolar variation in solute concentration, $k_B T$ is the thermal energy, R is the drop radius, K is the Gibbs adsorption length, and γ is the interfacial tension. Whether the drop becomes prolate or oblate depends on whether the solute–drop interaction is attractive or repulsive. Therefore, our work shows that in principle, a drop could undergo deformation during diffusiophoresis in a non-uniform solute gradient.

Key words: colloids, drops

1. Introduction

Phoretic motion refers to phenomena where a particle is moved by an external field, such as an electric field in electrophoresis (Morrison 1970), or a temperature gradient in thermophoresis (Young, Goldstein & Block 1959). In diffusiophoresis, a particle is

† Email address for correspondence: akhair@andrew.cmu.edu

© The Author(s), 2022. Published by Cambridge University Press

https://doi.org/10.1017/jfm.2022.666 Published online by Cambridge University Press

moved due to a solute concentration gradient: the motion is animated by an interactive force between the particle and solute molecules. Diffusiophoresis can occur in neutral (Ruckenstein 1981; Anderson, Lowell & Prieve 1982; Keh & Wang 2001; Marbach, Yoshida & Bocquet 2020) or electrolyte (Prieve, Ebel & Lowell 1984; Baygents & Saville 1988; Yang, Shin & Stone 2018; Marbach *et al.* 2020; Warren 2020) solutes. Diffusiophoretic particle speeds of the order of 1–10 μm s^{-1} are common (Velegol *et al.* 2016). Therefore, a spherical particle of radius 10 μm undergoing diffusiophoresis in water has a Reynolds number of the order 10^{-4}–10^{-5}, placing this phenomenon comfortably in the Stokes flow regime.

First elucidated by Derjaguin *et al.* (1947), the mechanism of diffusiophoresis was established further by Anderson, Prieve, and coworkers during the 1980s (Anderson *et al.* 1982; Prieve *et al.* 1984; Anderson 1989; Anderson & Prieve 1990). Interest has been renewed over the last decade or so due to microfluidic techniques enabling controlled experimental observation (Abécassis *et al.* 2009; Palacci *et al.* 2012; Shin *et al.* 2016; Nery-Azevedo, Banerjee & Squires 2017). Solute gradients capable of driving diffusiophoresis also occur in biological systems (Sear 2019; Ramm *et al.* 2021). Diffusiophoresis has been found to play a role in membrane fouling (Velegol *et al.* 2016) and fabric cleaning (Shin, Warren & Stone 2018). Diffusiophoresis also presents opportunities to induce microfluidic separations (Shin 2020), to deliver particles into dead-end pores (Kar *et al.* 2015; Ault *et al.* 2017), and to affect self-propulsion of microscale colloids (Paxton *et al.* 2004; Moran & Posner 2017; Decayeux *et al.* 2021).

A recent paper (Marbach *et al.* 2020) revisited the prototypical problem of diffusiophoresis of a solid particle in a uniform gradient of neutral solute. This problem has been considered previously by Anderson *et al.* (1982), who calculated the velocity at which a spherical particle translates. The velocity is found by requiring that the net, or 'global', force on the particle is zero, such that the hydrodynamic and the solute-interactive stresses integrated over the particle surface sum to zero. Marbach *et al.* (2020) extended this study to determine the distribution of stress over the particle surface, finding that the 'local' stress, which also includes hydrodynamic and solute-interactive contributions, is generally non-zero and non-uniform across the drop surface. Anderson *et al.* (1982) had previously found the translational velocity of the particle using the far-field decay of the velocity disturbance during its motion; that is, they did not need to compute the stress distribution over the particle surface. Due to the non-uniform stress, Marbach *et al.* (2020) suggested that a deformable particle subjected to these local stresses would lose its spherical shape. In turn, this would affect the translational velocity, i.e. diffusiophoresis of a deformable object is an inherently nonlinear problem due to this fluid–structure coupling. Marbach *et al.* (2020) proposed that this effect could be exploited to enable 'capillary diffusiophoresis' separations that would not require a gel medium like capillary electrophoresis, owing to the shape–velocity coupling of a deformable object undergoing diffusiophoresis. Motivated by the interesting analysis of Marbach *et al.* (2020), here we study the diffusiophoresis of a viscous drop in a neutral-solute gradient, a drop being a simple case of a deformable particle. We find that a drop undergoing diffusiophoretic motion in Stokes flow in a uniform solute gradient has no tendency to deform, regardless of the value of interfacial tension at the interface of the drop with its suspending fluid. This result is analogous to the absence of deformation for a sedimenting drop in Stokes flow (Taylor & Acrivos 1964). Consequently, we calculate the deformation caused by a non-uniform solute gradient and find that a quadratically varying solute distribution does lead, in principle, to drop deformation.

https://doi.org/10.1017/jfm.2022.666 Published online by Cambridge University Press

In § 2 we present the equations governing the solute distribution and fluid flow inside and outside a spherical viscous drop in a non-uniform gradient of non-ionic solute. We conduct a scaling analysis and non-dimensionalization of these coupled equations in § 3, which allows us to proceed asymptotically for small solute–drop interaction lengths. In § 4, using small-deformation theory for a small capillary number, $Ca \ll 1$, the surface stress distribution on an undeformed (spherical) drop is used to find the drop deformation to first order in Ca. We find in (4.18) that in a uniform solute gradient, the surface stresses cancel such that zero deformation occurs, in fact, for all orders of Ca. For the quadratic component of the solute field, we find a spheroidal shape to first order in Ca, given in the result (4.36). A discussion is given in § 5, which includes an examination of the physical conditions necessary for an observable deformation of a drop undergoing diffusiophoresis.

2. Governing equations

Existing theories of diffusiophoresis consider particle motion in a uniform solute gradient. The prescription of a uniform gradient is an inherently local approximation, since the solute concentration must be non-negative everywhere. The validity of this approximation is contingent on the length scale of the concentration gradient being large compared to the length scale of the particle. Further, one can conceive of numerous situations in which solute gradients can be non-uniform. Therefore, generally, at any point in a field of solute, the concentration distribution can be expanded as a series in terms of the growing spherical harmonics. Hence the undisturbed concentration distribution in the absence of an immersed object (in our case a drop) is given by

$$C_\infty(\boldsymbol{r}) = \chi + \alpha z + \beta\,\frac{3z^2 - r^2}{2} + O(r^3), \tag{2.1}$$

where r is the radial distance from the drop centre (i.e. the origin), and z is the Cartesian direction that defines the direction of drop translation (figure 1). Let θ be the polar angle formed with the positive z-axis, such that $z = r\cos\theta$. We define $\chi = C_\infty(\boldsymbol{0})$ as the uniform bulk concentration evaluated at the origin, $\alpha = |(\boldsymbol{\nabla} C_\infty)|_{\boldsymbol{r}=\boldsymbol{0}}$ as the uniform concentration gradient – only these first two terms are considered in existing studies of diffusiophoresis – and $\beta = |(\boldsymbol{\nabla}\boldsymbol{\nabla} C_\infty)|_{\boldsymbol{r}=\boldsymbol{0}}$ as the magnitude of the quadrupolar component of the solute field, which encapsulates the non-uniformity of the solute gradient. Due to symmetry, this quadrupolar contribution does not drive particle translation, but it does, as we will see, give rise to deformation of a drop. This quadrupolar contribution has not been studied previously, to our knowledge, either theoretically or experimentally. Undoubtedly, to set up a precise quadrupolar gradient in an experiment would be non-trivial. Perhaps one approach would be to adapt the 'soluto-inertial beacons' developed by Banerjee *et al.* (2016) that emit solute steadily over long time scales to affect diffusiophoretic transport of suspended colloids. One could imagine a set-up of four beacons at the corners of a square, where the top left and bottom right beacons emit solute, and the top right and bottom left beacons consume solute. This would result in a quadratic concentration variation near the centre of the square.

The presence of a drop creates a disturbance in this surrounding solute field due to the impenetrability of the drop to solute and due to the interactive forces between the solute and the drop. We will denote the interactive potential between the solute and the drop by ϕ, such that $-\boldsymbol{\nabla}\phi$ is the force exerted by the drop on a solute molecule at a position $\boldsymbol{r}$ from the drop centre. We assume that ϕ is a function of solely $r = |\boldsymbol{r}|$. We also assume that the interactive length L, which defines the distance from the drop surface beyond which

https://doi.org/10.1017/jfm.2022.666 Published online by Cambridge University Press

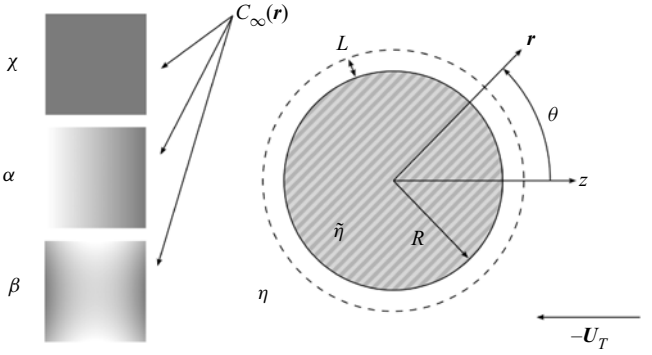


Figure 1. Definition sketch. A neutrally buoyant, spherical fluid drop of radius R is located at the origin of a frame of reference translating at the diffusiophoretic velocity $\boldsymbol{U}_T$. The position vector $\boldsymbol{r}$ extends from the drop centroid. The Cartesian coordinate z is the direction of the applied concentration gradient and serves as an axis around which the problem is symmetric. The polar angle θ is defined such that the z-axis is found at $\theta = 0$. The viscosities of the outer and inner fluids are given, respectively, by η and $\tilde{\eta}$. The drop, which contains no solute, interacts with a surrounding solute over an interactive length scale L. The drop is placed in a local undisturbed solute concentration field C_∞ that is approximated as a series expansion in the spherical harmonics. The first three components in the expansion (χ, α and β) represent the magnitudes of a uniform bulk concentration, a uniform solute gradient, and a quadrupolar distribution of solute, respectively.

interactions are negligible, is much smaller than the drop radius R. Following Anderson *et al.* (1982), we define $\lambda \equiv L/R$.

Modelling of diffusiophoresis requires solving coupled equations. Due to solute–drop interactions, the solute profile drives fluid flow, which in turn changes the solute concentration profile through advective fluxes. In the absence of bulk reactions, the concentration in terms of solute number density, C, satisfies the conservation equation

$$\frac{\partial C}{\partial t} = -\boldsymbol{\nabla}\cdot\boldsymbol{j} = \boldsymbol{\nabla}\cdot\left(D\,\boldsymbol{\nabla}C + \frac{D}{k_BT}\,C\,\boldsymbol{\nabla}\phi - C\boldsymbol{u}\right), \tag{2.2}$$

where $\boldsymbol{j}$ is the solute flux density, D is the solute diffusivity, k_BT is the thermal energy, and $\boldsymbol{u}$ is the fluid velocity. The three terms of this flux represent, from left to right respectively in (2.2), the fluxes due to diffusion, solute-drop interactive forces, and advection. We assume that solute cannot enter the drop. At distances far from the drop, the concentration field must return to the undisturbed form (2.1).

Consider a neutrally buoyant spherical drop for which all solute is confined to the exterior suspending fluid. The frame of reference will take the drop centre as its origin and will move with the yet unknown translational velocity $\boldsymbol{U}_T = U_T\widehat{\boldsymbol{e}}_z$, where $\widehat{\boldsymbol{e}}_z$ is the unit vector in the z-direction. Recall that the flux $\boldsymbol{j}$ in (2.2) includes an advective contribution, $C\boldsymbol{u}$. Hence when the drop has attained a steady shape, the no-flux condition is $\boldsymbol{n}\cdot\boldsymbol{j} = \boldsymbol{n}\cdot[\boldsymbol{\nabla}C + C\,\boldsymbol{\nabla}(\phi/k_BT)] = 0$, since $\boldsymbol{n}\cdot\boldsymbol{u} = 0$ by virtue of the impermeability of the drop interface to exterior or interior fluid. Considering the micron length scale of typical particles in diffusiophoresis, we assume that fluid flow is governed by the quasi-steady Stokes equations. The momentum balance in the exterior fluid has an added body force term $-C\,\boldsymbol{\nabla}\phi$ from drop–solute interactions. Denoting variables in the interior fluid with a tilde, we have a paired set of incompressible Stokes equations governing flow:

$$\eta\,\nabla^2\boldsymbol{u} - \boldsymbol{\nabla}p - C\,\boldsymbol{\nabla}\phi = 0, \quad \boldsymbol{\nabla}\cdot\boldsymbol{u} = 0, \tag{2.3a}$$

$$\tilde{\eta}\,\nabla^2\tilde{\boldsymbol{u}} - \boldsymbol{\nabla}\tilde{p} = 0, \quad \boldsymbol{\nabla}\cdot\tilde{\boldsymbol{u}} = 0, \tag{2.3b}$$

https://doi.org/10.1017/jfm.2022.666 Published online by Cambridge University Press

where η is the fluid viscosity, and p is the pressure. We assume that the interface is impenetrable to fluid:

$$\boldsymbol{n}\cdot\boldsymbol{u}=\boldsymbol{n}\cdot\widetilde{\boldsymbol{u}}=0\quad\text{at } r=R. \tag{2.4}$$

We also assume the no-slip condition (Leal 2007)

$$\boldsymbol{n}\times\boldsymbol{u}=\boldsymbol{n}\times\widetilde{\boldsymbol{u}}\quad\text{at } r=R. \tag{2.5}$$

To ensure finite velocity everywhere, we set the limiting conditions

$$\boldsymbol{u}\to-U_T\widehat{\boldsymbol{e}}_z \text{ as } r\to\infty,\quad \widetilde{\boldsymbol{u}} \text{ is finite as } r\to 0. \tag{2.6}$$

Next, we consider the stress balance on the drop interface. The effects on the interface are due to the hydrodynamic stress, solute-interactive stress and surface tension, which give the balance

$$\left[\boldsymbol{\Pi}-\tilde{\boldsymbol{\Pi}}\right]\cdot\boldsymbol{n}+\boldsymbol{\Sigma}=\gamma\boldsymbol{n}\,\nabla\cdot\boldsymbol{n}\quad\text{at } r=R, \tag{2.7}$$

where $\boldsymbol{\Pi}=-p\boldsymbol{I}+\eta(\nabla\boldsymbol{u}+(\nabla\boldsymbol{u})^{\mathrm{T}})$ and $\tilde{\boldsymbol{\Pi}}$ are the Newtonian fluid stress tensors, $\boldsymbol{I}$ is the identity tensor, the solute-interactive stress $\boldsymbol{\Sigma}$ captures the solute-interactive forces exerted upon a differential area element on the drop interface, and γ is the surface tension. We do not allow explicitly for variations in the surface tension γ along the drop surface, which would give rise to a Marangoni stress jump. To quantify the solute-interactive stress locally, consider that each solute molecule exerts a normal force $\nabla\phi$ on that surface element, which can be summed by integrating $C\,\nabla\phi$ over a volume extending from that element on the interface (Marbach *et al.* 2020). As a sum of normal forces per unit area, $\boldsymbol{\Sigma}$ is also normal, thus $\boldsymbol{\Sigma}=\boldsymbol{n}\Sigma$. This interactive volume, on a spherical interface, takes the form of a truncated cone extending outwards from a surface element $\mathrm{d}A$, since in this case the external differential volume element is given by $\mathrm{d}V=(r/R)^2\,\mathrm{d}r\,\mathrm{d}A$. Hence the net solute-interactive stress on a surface element $\mathrm{d}A$ has magnitude

$$\Sigma=\int_R^\infty C\frac{\mathrm{d}\phi}{\mathrm{d}r}\left(\frac{r}{R}\right)^2\mathrm{d}r. \tag{2.8}$$

Since the solute-interactive stress and surface tension act in the normal direction, the tangential stress balance is solely hydrodynamic:

$$\boldsymbol{n}\times(\boldsymbol{\Pi}\cdot\boldsymbol{n})=\boldsymbol{n}\times\left(\tilde{\boldsymbol{\Pi}}\cdot\boldsymbol{n}\right)\quad\text{at } r=R. \tag{2.9}$$

The tangential stress balance is not solely hydrodynamic in electrophoresis, as noted by Marbach *et al.* (2020); in that case, the electric (Maxwell) stress in an electrolyte (i.e. a non-neutral ionic solute) contains a tangential component. Thus for diffusiophoresis in an electrolyte, one would also have a Maxwell stress contribution to the tangential stress balance.

The translational velocity $\boldsymbol{U}_T$, an unknown in the flow problem, can be found by balancing the hydrodynamic and solute-interactive stress integrated across the entire drop surface, ensuring a global equilibrium between the forces exerted on the drop by the suspending solution. The total solute-interactive stress is quantified by the sum of interactive forces $\nabla\phi$ exerted by solute molecules in the entire volume exterior to the drop, V_{out}, which thereby yields the global force balance

$$\iint_{r=R}(\boldsymbol{n}\cdot\boldsymbol{\Pi}+\boldsymbol{\Sigma})\,\mathrm{d}A=\iint_{r=R}\boldsymbol{n}\cdot\boldsymbol{\Pi}\,\mathrm{d}A+\iiint_{V_{out}}C\,\nabla\phi\,\mathrm{d}V=\boldsymbol{0}. \tag{2.10}$$

https://doi.org/10.1017/jfm.2022.666 Published online by Cambridge University Press

3. Scaling of the problem

The solute and flow problems in § 2 are nonlinearly coupled. To make analytical progress, we begin with a scaling analysis. We scale the time by R^2/D (which represents the characteristic time for a solute molecule to diffuse across the drop radius), the distance by the particle radius R, and the velocity by a scale U that is to be determined. We denote scaled variables with an asterisk, and the dimensionless interactive potential function $\phi^* = \phi/k_BT$ is normalized by the thermal energy. The advection–diffusion equation (2.2) can then be written as

$$\frac{\partial C}{\partial t^*} = \nabla^* \cdot \left(\nabla^* C + C\,\nabla^* \phi^* - Pe\, C\boldsymbol{u}^*\right), \tag{3.1}$$

where the Péclet number is $Pe = RU/D$. We will make the common assumption that advection is negligible compared to the other terms, which is true when the diffusive time scale R^2/D is much smaller than the convective time scale R/U. This is characterized by a low Péclet number ($Pe \ll 1$). This assumption eliminates the nonlinear coupling, enabling us to solve the disturbed solute distribution independent of the fluid flow. Neglecting solute advection also allows us to solve the disturbed solute distribution and the resulting fluid flow caused by the imposed uniform solute gradient separately from those caused by the imposed quadrupolar solute gradient, through linear superposition. For studies on the effect of solute advection in diffusiophoresis, see, for example, Anderson & Prieve (1990), Keh & Wang (2001), Khair (2013) and Michelin & Lauga (2014).

In a frame of reference moving at the translational speed U_T, a time dependence is introduced into the far-field condition for the solute field:

$$C \to \chi + \alpha U_T t + \beta\,(U_T t)^2 + (\alpha + 2\beta U_T t)\,z + \beta\,\frac{3z^2 - r^2}{2} \quad \text{as } r \to \infty. \tag{3.2}$$

This time dependence can be neglected if the time scale for a significant change in the concentration to occur is much shorter than the diffusive time scale for the solute profile to relax into a pseudo-steady state. Combined with the condition of low Péclet number, it requires that $\alpha \lesssim \chi/R$ and $\beta \lesssim \alpha/2R$. Under these conditions, the far-field concentration can be set to (2.1), and (3.1) can be solved in a pseudo-steady state, with a solution of the form

$$C = \chi\, W(r) + \alpha R\, P(r)\cos\theta + \beta R^2\, Q(r)\,\frac{3\cos^2\theta - 1}{2}, \tag{3.3}$$

where we have defined $W(r)$, $P(r)$ and $Q(r)$ as functions capturing the radial dependence of each component of the disturbed solute concentration distribution. The functions $P(r)$ and $Q(r)$ are named in analogy to electrostatics as a concentration dipole and quadrupole. Substituting (3.3) into (3.1) allows us to write separate equations for each component of the imposed solute field. Forbidding solute flux at the interface ($\boldsymbol{n}\cdot\boldsymbol{j} = 0$), we obtain the following governing equations for the radial dependence of the disturbed solute concentration, separated by angular dependence: the angularly independent bulk concentration satisfies

$$\left[\rho^2\left(W'(\rho) + W(\rho)\,\frac{\mathrm{d}\phi^*}{\mathrm{d}\rho}\right)\right]' = 0, \tag{3.4a}$$

$$W'(\rho) + W(\rho)\,\frac{\mathrm{d}\phi^*}{\mathrm{d}\rho} = 0 \text{ at } \rho = 1, \quad W \to 1 \text{ as } \rho \to \infty, \tag{3.4b}$$

where $\rho \equiv r/R$ is a scaled radial coordinate, and the prime will denote derivatives with respect to ρ henceforth. The governing equation for the radial component of the uniform

https://doi.org/10.1017/jfm.2022.666 Published online by Cambridge University Press

gradient, as formulated by Anderson *et al.* (1982), is given by

$$P''(\rho)+\left(\frac{\mathrm{d}\phi^*}{\mathrm{d}\rho}+\frac{2}{\rho}\right)P'(\rho)+\left(\frac{\mathrm{d}^2\phi^*}{\mathrm{d}\rho^2}+\frac{2}{\rho}\frac{\mathrm{d}\phi^*}{\mathrm{d}\rho}-\frac{2}{\rho^2}\right)P(\rho)=0, \tag{3.5a}$$

$$P'(\rho)+P(\rho)\frac{\mathrm{d}\phi^*}{\mathrm{d}\rho}=0 \text{ at } \rho=1, \quad P\to\rho \text{ as } \rho\to\infty. \tag{3.5b}$$

Note that a uniform gradient can be viewed as an imposed dipole variation in concentration. Finally, the radial dependence of the quadrupolar solute distribution is governed by

$$Q''(\rho)+\left(\frac{\mathrm{d}\phi^*}{\mathrm{d}\rho}+\frac{2}{\rho}\right)Q'(\rho)+\left(\frac{\mathrm{d}^2\phi^*}{\mathrm{d}\rho^2}+\frac{2}{\rho}\frac{\mathrm{d}\phi^*}{\mathrm{d}\rho}-\frac{6}{\rho^2}\right)Q(\rho)=0, \tag{3.6a}$$

$$Q'(\rho)+Q(\rho)\frac{\mathrm{d}\phi^*}{\mathrm{d}\rho}=0 \text{ at } \rho=1, \quad Q\to\rho^2 \text{ as } \rho\to\infty. \tag{3.6b}$$

Next, the velocity fields can be solved by defining axisymmetric Stokes stream functions ψ and $\tilde{\psi}$ such that

$$\boldsymbol{u}=\frac{\widehat{\boldsymbol{e}}_\varphi}{\rho\sin\theta}\times\boldsymbol{\nabla}^*\psi(r,\theta), \quad \tilde{\boldsymbol{u}}=\frac{\widehat{\boldsymbol{e}}_\varphi}{\rho\sin\theta}\times\boldsymbol{\nabla}^*\tilde{\psi}(r,\theta), \tag{3.7a,b}$$

where $\widehat{\boldsymbol{e}}_\varphi$ is the spherical coordinate unit vector in the azimuthal direction. The incompressibility conditions in (2.3) are satisfied automatically by this representation. Due to the linearity of the Stokes equations, the velocity can also be expressed as a sum of the fluid flows induced by each component of the solute gradient. The uniform concentration χ induces no flow, however. The angular dependencies of the dipole- and quadrupole-induced flows are satisfied by decomposing the stream functions as

$$\psi=U_\alpha\,\psi_\alpha(\rho)\sin^2\theta+U_\beta\,\psi_\beta(\rho)\sin^2\theta\cos\theta, \tag{3.8a}$$

$$\tilde{\psi}=U_\alpha\,\tilde{\psi}_\alpha(\rho)\sin^2\theta+U_\beta\,\tilde{\psi}_\beta(\rho)\sin^2\theta\cos\theta, \tag{3.8b}$$

where $U_\alpha\equiv\alpha R^2k_BT/\eta$ and $U_\beta\equiv\beta R^3k_BT/\eta$ are velocity scales found by normalizing the decomposed Stokes equations. In (3.8), ψ_α and ψ_β denote the radially dependent components of the stream functions of the dipole- and quadrupole-induced flows, respectively. We then apply (3.7*a*,*b*) and (3.8) to the Stokes equations (2.3). For the uniform gradient, we recover the dipole-induced flow problem as posed in Anderson *et al.* (1982):

$$E^4\psi_\alpha=\frac{\mathrm{d}\phi^*}{\mathrm{d}\rho}P(\rho), \quad E^4\tilde{\psi}_\alpha=0, \tag{3.9a,b}$$

$$\psi_\alpha=\tilde{\psi}_\alpha=0, \quad \psi_\alpha'=\tilde{\psi}_\alpha', \quad \left(\psi_\alpha'/\rho^2\right)'=\sigma\left(\tilde{\psi}_\alpha'/\rho^2\right)' \text{ at } \rho=1, \tag{3.9c,d,e}$$

$$\psi_\alpha\to\frac{1}{2}U_T^*\rho^2 \text{ as } \rho\to\infty, \quad \tilde{\psi}_\alpha/\rho^2 \text{ is finite as } \rho\to0, \tag{3.9f,g}$$

$$\lim_{\rho\to\infty}\left[\frac{1}{\rho}\left(\psi_\alpha-\frac{1}{2}U_T^*\rho^2\right)\right]=0, \tag{3.9h}$$

where U_T^* is the translational velocity scaled by U_α, σ is the viscosity ratio $\tilde{\eta}/\eta$, E^2 is the operator $E^2=\partial^2/\partial\rho^2-2/\rho^2$, and (3.9*h*) is the force-balance condition in terms of

https://doi.org/10.1017/jfm.2022.666 Published online by Cambridge University Press

the stream function. This last condition stipulates that at large distances from the drop ($\rho \gg 1$), where solute-interactive forces are negligible, the velocity decay must be more rapid than a Stokeslet ($\sim 1/\rho$). In the quadrupolar case, no condition equivalent to (3.9*h*) is needed, since the drop is not expected to translate on grounds of symmetry. The problem for this component of the stream function is given by

$$\left(\psi_\beta''' - \frac{12}{\rho^2}\,\psi_\beta'\right)' = 3\,\frac{\mathrm{d}\phi^*}{\mathrm{d}\rho}\,Q(\rho), \quad \left(\tilde{\psi}_\beta''' - \frac{12}{\rho^2}\,\tilde{\psi}_\beta'\right)' = 0, \tag{3.10a,b}$$

$$\psi_\beta = \tilde{\psi}_\beta = 0, \quad \psi_\beta' = \tilde{\psi}_\beta', \quad \left(\psi_\beta'/\rho^2\right)' = \sigma\left(\tilde{\psi}_\beta'/\rho^2\right)' \text{ at } \rho = 1, \tag{3.10c,d,e}$$

$$\psi_\beta \to 0 \text{ as } \rho \to \infty, \quad \tilde{\psi}_\beta/\rho^2 \text{ is finite as } \rho \to 0. \tag{3.10f,g}$$

3.1. *Small deformation theory*

Following the domain perturbation method described by Leal (2007), we can calculate the shape of a slightly deformed drop in the limit of small capillary number $Ca \equiv \eta U/\gamma$, a dimensionless group comparing viscous forces ηUR to surface tension forces γR. When surface tension dominates ($Ca \ll 1$), drop deformation is accordingly small. In this limit, we can expand the drop shape as a perturbation series in Ca, where the leading-order solution is the undeformed, or spherical, shape. The boundary conditions at the actual (deformed) surface of the drop are transferred onto the undeformed (spherical) surface at $\rho = 1$ by exploiting the assumed smallness of the deformation. Thus the leading-order solute and flow fields, i.e. at $O(Ca^0)$ or $O(1)$, are subject to the boundary conditions around an undeformed (spherical) drop. This leading-order solution is then used to calculate the deformation to first order in the capillary number Ca via the normal stress balance. Continuing the technique to higher orders in Ca would require the boundary conditions at $\rho = 1$ to account for the deformation of the drop; consequently, the algebraic complexity would increase rapidly. In this work, we calculate only the first-order deformation.

The surface of the drop is parametrized by defining a level set function $S = 0$ and a function f that represents the $O(Ca)$ deviation from sphericity:

$$S(\boldsymbol{r}) \equiv r - R\left[1 + Caf(\boldsymbol{r})\right] \equiv 0. \tag{3.11}$$

For $Ca \to 0$, the shape is spherical, as expected. For a sphere, the surface normal vector is simply $\widehat{\boldsymbol{e}}_r$, but for the deformed shape defined above, the normal vector is

$$\boldsymbol{n} \equiv \frac{\boldsymbol{\nabla} S}{|\boldsymbol{\nabla} S|} = \widehat{\boldsymbol{e}}_r - Ca\,\boldsymbol{\nabla}_s^* f + O(Ca^2), \tag{3.12}$$

where $\boldsymbol{\nabla}_s^* = (\boldsymbol{I} - \widehat{\boldsymbol{e}}_r\widehat{\boldsymbol{e}}_r)\cdot\boldsymbol{\nabla}^*$ is the surface gradient operator on a sphere. The leading-order solution is then solved around a spherical geometry. Recognizing that for this undeformed case the solute concentration profiles and flow profiles are superimposed linearly with different angular dependencies and concentration scalings (χ, αR and βR^2), we can separate the terms in the leading-order normal stress jump, $\Pi_{rr} - \tilde{\Pi}_{rr} + \Sigma$, based on their angular dependencies. That is, we write

$$\Sigma \equiv \Sigma^\chi + \Sigma^\alpha \cos\theta + \Sigma^\beta\,\frac{3\cos^2\theta - 1}{2}, \tag{3.13a}$$

$$\Pi_{rr} - \tilde{\Pi}_{rr} \equiv \Pi_{rr}^\chi - \tilde{\Pi}_{rr}^\chi + \left[\Pi_{rr}^\alpha - \tilde{\Pi}_{rr}^\alpha\right]\cos\theta + \left[\Pi_{rr}^\beta - \tilde{\Pi}_{rr}^\beta\right]\frac{3\cos^2\theta - 1}{2}. \tag{3.13b}$$

https://doi.org/10.1017/jfm.2022.666 Published online by Cambridge University Press

Corrections to these leading-order stresses due to first-order deformations do not participate in the calculation of the deformation to $O(Ca)$. Each of these stress components is associated with a different velocity scaling, one of which must be chosen in order to define a capillary number $Ca = \eta U/\gamma$. The solute-interactive stress Σ in each case is of the same scaling as the associated hydrodynamic normal stress jump, $\Pi_{rr} - \tilde{\Pi}_{rr}$, since the solute-interactive forces are responsible for the fluid flow. As will be shown in § 4.2, the imposed dipole concentration field (i.e. uniform gradient), though it induces a stronger flow than the imposed quadrupolar field (i.e. the non-uniform gradient), contributes no deformative effect to the drop shape. Therefore, the characteristic velocity pertaining to deformation comes from the quadrupole-induced flow, and the velocity scale is chosen to be $U_\beta = \beta R^3 k_B T/\eta$; hence $Ca = \beta R^3 k_B T/\gamma$. We scale the stress tensor and interactive stress by $\eta U_\beta/R$ $(= \beta R^2 k_B T)$. Denoting the scaled quantities with an asterisk, we obtain the dimensionless form of the normal component of the stress balance (2.7) as

$$\Pi^*_{rr} - \sigma\tilde{\Pi}^*_{rr} + \Sigma^* + O(Ca) = \frac{1}{Ca}\nabla^* \cdot \boldsymbol{n}, \tag{3.14}$$

where again σ is the viscosity ratio, and the $O(Ca)$ corrections to the normal stress jump have been omitted. The mismatch to first order in Ca between the normal stress jump and surface tension effects (the right-hand side of (3.14)) provides the opportunity to perturb the drop surface as a Taylor series for $Ca \ll 1$. Substituting the normal vector (3.12) into the normal stress balance (3.14) yields

$$\Pi^*_{rr} - \sigma\tilde{\Pi}^*_{rr} + \Sigma^* = \frac{2}{Ca} - \nabla^{*2}_s f + O(Ca). \tag{3.15}$$

In order to find f, first notice that f is linearly related to the dynamic variables $\boldsymbol{u}$, $\widetilde{\boldsymbol{u}}$, and the normal stresses. Since f is a true scalar, it must be – like these dynamic variables – linearly related to the dipole and quadrupole components of the imposed concentration gradients $\alpha r\cos\theta$ and $\beta r^2(3\cos^2\theta - 1)/2$. Thus we decompose f on the spherical interface as

$$f(\theta) = \delta_\alpha \cos\theta + \delta_\beta \frac{3\cos^2\theta - 1}{2}, \tag{3.16}$$

where δ_α and δ_β are dimensionless constants characterizing the magnitude of deformation due to the dipole- and quadrupole-imposed solute fields, respectively. These values can then be found by matching the leading-order normal stress jump in (3.15). But to do so we must first solve for the solute and flow fields around a spherical drop, which is pursued next.

4. Results and discussion

4.1. *Uniform solute concentration*

First, we find by solving (3.4) that the effect of solute–drop interactions on a uniform solute concentration χ is

$$W(r) = \chi \exp\left(-\phi^*(r)\right), \tag{4.1}$$

where the Boltzmann factor describes spatial variation of the solute concentration within the interactive region due to attraction or repulsion of the uniform bulk concentration. There is no flow induced by the uniform solute field, due to spherical symmetry. Thus the

https://doi.org/10.1017/jfm.2022.666 Published online by Cambridge University Press

only contributor to hydrodynamic stress is the osmotic pressure in the exterior fluid p^{χ}, which varies based on solute attraction or repulsion:

$$p^{\chi}(r) = p_0 + k_B T \chi [\exp(-\phi^*(r)) - 1], \tag{4.2}$$

where p_0 is the solution pressure in the absence of the drop. The value of p_0 is arbitrary because the fluid is incompressible. We can then evaluate the interactive stress exerted on the interface by the uniform bulk solute, Σ^{χ}, from (2.8). We define an inner coordinate scaled to the interaction length as $y \equiv (r - R)/L = (r/R - 1)/\lambda$, where y is $O(1)$ in the interactive region. By converting the radial coordinate r to y and using integration by parts, we obtain

$$\begin{aligned}\Sigma^{\chi} &= \int_0^{\infty} k_B T \chi \exp(-\phi^*) \frac{\mathrm{d}\phi^*}{\mathrm{d}y} (1 + \lambda y)^2 \mathrm{d}y \\ &= k_B T \chi \left\{ [\exp(-\phi^*(R)) - 1] + 2 \frac{K}{L} \left(\lambda + \lambda^2 \frac{I}{L} \right) \right\},\end{aligned} \tag{4.3}$$

where K is the adsorption length associated with the excess solute concentration drawn towards or repelled from the drop surface, given by

$$K \equiv \int_R^{\infty} [\exp(-\phi^*(r)) - 1] \mathrm{d}r, \tag{4.4}$$

and I is another length, defined by

$$I \equiv K^{-1} \int_R^{\infty} r [\exp(-\phi^*(r)) - 1] \mathrm{d}r. \tag{4.5}$$

As discussed in Anderson *et al.* (1982), this length I is the same order of magnitude as the interaction length L for a wide variety of potential functions (e.g. square-well, exponential, Lennard-Jones). With these stresses calculated, we then turn to the normal stress balance (3.15); considering the angularly independent effects in this balance, we obtain

$$\tilde{p}_0 - p_0 = \gamma \frac{2}{R} - 2 k_B T \chi \frac{K}{R} \left(\frac{R + I}{R} \right), \tag{4.6}$$

where $\tilde{p}_0$ is the equilibrium pressure inside the drop. For an attractive drop–solute interaction ($K > 0$), the pressure jump is lessened, and for a repulsive interaction ($K < 0$), the pressure jump is increased. At equilibrium, the adsorption length K can be related to the surface tension via the Gibbs equation

$$K = \frac{\Gamma}{\chi} = -\frac{1}{k_B T} \left(\frac{\partial \gamma}{\partial \chi} \right)_T, \tag{4.7}$$

where Γ is the Gibbs surface excess concentration, a measurable quantity. Applying the Gibbs equation (4.7) to (4.6), we obtain

$$\tilde{p}_0 - p_0 = \frac{2}{R} \left[\gamma + \chi \left(\frac{\partial \gamma}{\partial \chi} \right)_T \left(\frac{R + I}{R} \right) \right]. \tag{4.8}$$

As mentioned above, the length I is typically much smaller than the drop radius R. Consequently, in (4.8) $(R + I)/R \to 1$, and the resulting modified Young–Laplace equation accounts for the effect of solute–particle interactions on the effective interfacial tension of the drop. Thus in the limit $I/R \to 0$, the effect of the solute on the stress jump is equivalent to a surface contaminant, or surfactant, modifying the interfacial tension. We have neglected the possibility of deformation through a uniform change in the drop radius, as this would violate the incompressibility of the fluids.

https://doi.org/10.1017/jfm.2022.666 Published online by Cambridge University Press

4.2. *Uniform solute gradient*

Now we consider the effects of the uniform solute gradient α, beginning with the disturbed solute profile. Due to the different physical balances between the inner region ($\rho - 1 \lesssim \lambda$), where solute–drop interactions play an important role, and the outer region ($\rho - 1 \gg \lambda$), where these interactions are negligible, we use asymptotic matching in terms of the small parameter λ, as detailed in Anderson *et al.* (1982). In the outer region, we solve (3.5) with ϕ^* set to zero. In the inner region, we use the inner coordinate y and solve (3.5), matching terms at each order in λ with the outer solution. Around a spherical drop, we find the following concentration profile:

$$P = \begin{cases} P^O(\rho) = \rho + \dfrac{1}{2}\rho^{-2}\left(1 - 3\,\dfrac{K}{L}\,\lambda + O(\lambda^2)\right) & \text{for } \rho - 1 \gg \lambda, \\ P^I(y) = \dfrac{3}{2}\left(1 - \dfrac{K}{L}\,\lambda + O(\lambda^2)\right)\exp\left(-\phi^*(y)\right) & \text{for } \rho - 1 \lesssim \lambda, \end{cases} \tag{4.9}$$

where the superscripts O and I indicate the solutions in the outer and inner regions, respectively. This dipolar profile P is given by Anderson *et al.* (1982) in their (2.22), and the reader is directed to their paper for a detailed derivation of (4.9).

Next, we solve for the flow field inside and outside the drop. Using variation of parameters to solve for $\psi_\alpha(\rho)$, we find the following exact solutions for the stream functions of the flows induced by the uniform gradient of solute

$$\psi_\alpha(\rho) = \frac{1}{3}\left[\xi_\alpha'(1) + \xi_\alpha(1) - \frac{\xi_\alpha''(1) - 2\,\xi_\alpha(1)}{2 + 3\sigma}\right]\left(\frac{1}{\rho} - \rho^2\right) + \xi_\alpha(\rho) - \frac{\xi_\alpha(1)}{\rho}, \tag{4.10a}$$

$$\tilde{\psi}_\alpha(\rho) = \frac{\xi_\alpha''(1) - 2\,\xi_\alpha(1)}{2(2 + 3\sigma)}\left(\rho^4 - \rho^2\right), \tag{4.10b}$$

where ξ_α, the particular solution of (3.9*a*,*b*), is given by

$$\xi_\alpha(\rho) = \frac{1}{6}\int_\rho^\infty \left[\frac{1}{5}\left(\frac{v^4}{\rho} - \frac{\rho^4}{v}\right) + \rho^2 v - v^2\rho\right] P(v)\,\frac{\mathrm{d}\phi^*}{\mathrm{d}v}\,\mathrm{d}v, \tag{4.11}$$

where v is a dummy outer variable. The result for the diffusiophoretic translation speed of a drop has been found in Anderson *et al.* (1982) (see their (4.11)) to leading asymptotic order under the thin layer ($\lambda \to 0$) assumption as

$$U_T \sim \frac{\alpha k_B T K}{\eta}\,\frac{3\sigma I + R}{3\sigma + 2}. \tag{4.12}$$

As mentioned above, the ratio I/R is typically much smaller than unity. For moderately viscous drops, such that $\sigma I/R \to 0$ as $I/R \to 0$, we have $U_T = \alpha k_B T K R/(\eta(3\sigma + 2))$. As noted by Anderson *et al.* (1982), this speed equals the speed of a drop in a gradient of a surface-active solute, or surfactant. Thus for a moderately viscous drop ($\sigma \lesssim 1$) in the limit $I/R \to 0$, the action of the solute distribution within the interfacial layer is equivalent to a Marangoni stress due to a variation in interfacial tension. However, the equivalence breaks down for highly viscous drops, $\sigma I/R \gg 1$, where the limiting behaviour is $U_T = \alpha k_B T K I/\eta$, which is that of a rigid particle undergoing diffusiophoresis. Here, the translation speed is independent of the particle size. In this regime, the diffuse nature of the stress in the thin interfacial region cannot be represented by a Marangoni stress at the literal drop interface,

https://doi.org/10.1017/jfm.2022.666 Published online by Cambridge University Press

We now obtain the hydrodynamic stresses on the drop surface. Recall that Anderson *et al.* (1982) did not need to do this when determining the translation speed of the drop. Using the Stokes equations, we find that the hydrodynamic normal stress jump on the interface can be written in terms of the stream functions as

$$\Pi^{\alpha}_{rr} - \tilde{\Pi}^{\alpha}_{rr} = \frac{\eta U_\alpha}{R}[(\psi'''_\alpha - \sigma\tilde{\psi}'''_\alpha) - 6(\psi'_\alpha - \sigma\tilde{\psi}'_\alpha) + 12(\psi_\alpha - \sigma\tilde{\psi}_\alpha)]_{\rho=1}. \tag{4.13}$$

By applying the solutions of the Stokes equations (4.10), this hydrodynamic stress jump can be expressed in terms of the particular solution ξ_α, and we find no dependence on the viscosity ratio σ in the following exact expression:

$$\Pi^{\alpha}_{rr} - \tilde{\Pi}^{\alpha}_{rr} = \frac{\eta U_\alpha}{R}\left(\xi'''_\alpha - 2\xi''_\alpha - 2\xi'_\alpha + 8\xi_\alpha\right)\Big|_{\rho=1}. \tag{4.14}$$

From (2.8), the interactive stress due to the uniform gradient is given by

$$\Sigma^{\alpha} = \frac{\eta U_\alpha}{R}\int_1^\infty \rho^2 \frac{\mathrm{d}\phi^*}{\mathrm{d}\rho} P(\rho)\,\mathrm{d}\rho. \tag{4.15}$$

By applying (3.9*a*,*b*), (4.15) can be rewritten as

$$\begin{aligned}\Sigma^{\alpha} &= \frac{\eta U_\alpha}{R}\int_1^\infty \rho^2 E^4 \psi_\alpha\,\mathrm{d}\rho \\ &= \frac{\eta U_\alpha}{R}\int_1^\infty \left(\rho^2\psi'''_\alpha - 2\rho\psi''_\alpha - 2\psi'_\alpha + \frac{8}{\rho}\psi_\alpha\right)'\mathrm{d}\rho.\end{aligned} \tag{4.16}$$

There is no contribution from the upper limit of the integral provided that ϕ^* decays faster than ρ^{-3} at large ρ. Under this assumption, we apply (4.10) and simplify terms that cancel out to obtain the exact expression

$$\Sigma^{\alpha} = -\frac{\eta U_\alpha}{R}(\xi'''_\alpha - 2\xi''_\alpha - 2\xi'_\alpha + 8\xi_\alpha)\Big|_{\rho=1}. \tag{4.17}$$

Thus we find the remarkable result that

$$\Pi^{\alpha}_{rr} - \tilde{\Pi}^{\alpha}_{rr} + \Sigma^{\alpha} = 0, \tag{4.18}$$

at each point on the interface. Therefore, the local hydrodynamic and solute-interactive normal stresses generated by the uniform gradient sum to zero. From (3.15), this means that a drop undergoing diffusiophoresis has no tendency to deform; that is,

$$\delta_\alpha = 0. \tag{4.19}$$

Reaching this result did not require assuming that the interactive layer is thin, since the asymptotic forms for the dipolar solute distribution P in (4.9) have not been invoked. Given (4.19), higher-order contributions in Ca to the shape function $f(\theta)$ must vanish. Therefore, in a uniform gradient, the drop has no tendency to deform, regardless of the value of Ca, as long as the Reynolds number is zero. Physically, this happens because the jump in the hydrodynamic stress across the interface cancels exactly the solute-interactive normal stress, as evident in (4.18). All that is left, then, is the jump in pressure due to uniform surface tension, i.e. the capillary stress, which is isotropic and hence causes no deformation. An analogous phenomenon occurs when a drop undergoes sedimentation at

https://doi.org/10.1017/jfm.2022.666 Published online by Cambridge University Press

zero Reynolds number, where the drop also has no tendency to deform (Taylor & Acrivos 1964). In sedimentation, the hydrodynamic normal stress cancels the buoyant normal stress jump across a drop. Of course, the flow fields around a drop undergoing diffusiophoresis and sedimentation are quite different. The hydrodynamic and gravitational forces on a drop balance in sedimentation, such that there is a net hydrodynamic force on the drop; in this sense, the drop is not 'force-free'. However, the total force (hydrodynamic plus gravitational) is zero, as is required by any motion at zero Reynolds number. Consequently, the velocity field far from the drop decays slowly like one over distance from the drop centroid, i.e. a Stokeslet, which is characteristic of any object on which a net hydrodynamic force is exerted. In diffusiophoresis, the total force is again zero, but here the total force is the sum of hydrodynamic and solute-interactive forces; if the latter are constrained to a thin interfacial layer (which is the limit that we consider), then on the drop scale, it appears that the drop moves as if the hydrodynamic force on it were zero. Consequently, the velocity field now decays much faster, like one over distance cubed, characteristic of a potential dipole. Despite these differences, however, it is the analogy in the normal stress balances that enables a linkage in the result of no deformation during diffusiophoresis in a uniform solute gradient and sedimentation in a uniform gravitational field. At non-zero Reynolds number, a drop undergoing sedimentation deforms due to inertial forces in the fluid (Taylor & Acrivos 1964). Thus we anticipate that deformation could occur for diffusiophoresis in a uniform solute gradient at non-zero Reynolds number. This could be relevant in the case of an air bubble undergoing diffusiophoresis, where the small viscosity inside the bubble causes the assumption of a zero-Reynolds-number interior flow to be questionable.

Equation (4.18) does not follow the prediction made by Marbach *et al.* (2020) that a deformable particle would deviate from sphericity during diffusiophoresis under a uniform solute gradient. Their prediction was based on the consideration of the local stress distribution on a rigid spherical particle. Our results can be interpreted as those for a rigid particle in the limit of infinite internal viscosity, $\sigma \to \infty$. We can then recover the rigid-particle stress distribution result of Marbach *et al.* (2020) (their (3.35)). To do this, we ignore the hydrodynamic stress from the interior of the drop, leaving

$$\Pi^{\alpha}_{rr} + \Sigma^{\alpha} = \frac{6\sigma}{2+3\sigma}\frac{\eta U_{\alpha}}{R}(\xi''_{\alpha} - 2\xi_{\alpha})\bigg|_{\rho=1}. \tag{4.20}$$

In the inner region of (4.9), the concentration profile can be expressed as the product of the Boltzmann factor with the outer-region solution, $P^{O}(\rho)$, evaluated approaching the inner region, that is,

$$P^{I}(y) = P^{O}(1)\exp(-\phi^{*}(y)), \tag{4.21}$$

where $P^{O}(1)$ is the outer-region solution evaluated at $\rho = 1$. Applying (4.21) to (4.11) and performing integration by parts, we obtain

$$\xi_{\alpha}(\rho) = \frac{P^{O}(1)}{6}\int_{\rho}^{\infty}\left[\frac{1}{5}\left(4\frac{v^3}{\rho} + \frac{\rho^4}{v^2}\right) + \rho^2 - 2v\rho\right][\exp(-\phi^{*}(v)) - 1]\mathrm{d}v. \tag{4.22}$$

Then, converting (4.22) into terms of the inner coordinate y and expanding asymptotically in λ yields

$$\xi_{\alpha}(y) = \frac{3}{2}\lambda^3\left(1 - \lambda\frac{K}{L}\right)\int_{y}^{\infty}\frac{(y-x)^2}{2}[\exp(-\phi^{*}(x)) - 1]\mathrm{d}x + O(\lambda^5), \tag{4.23}$$

where x is a dummy inner variable. Finally, by converting (4.20) to the inner coordinate y and applying (4.23), we recover the result of Marbach *et al.* (2020), which is given to

https://doi.org/10.1017/jfm.2022.666 Published online by Cambridge University Press

leading order in λ by

$$\lim_{\sigma\to\infty}\left[\left(\Pi^{\alpha}_{rr}+\Sigma^{\alpha}\right)\cos\theta\right]=3\alpha k_B TK\cos\theta. \tag{4.24}$$

Thus considering only the exterior fluid stress and the solute-interactive stress gives a non-zero, and non-uniform, local stress on the particle surface. However, inclusion of the interior stress leads to a zero local stress (4.18) at each point on the drop surface, which means that there is no tendency for the drop to deform. The conclusion, therefore, is that deformation cannot be predicted without consideration of internal stress.

4.3. *Non-uniform solute gradient*

Finding no deformation caused by the uniform gradient, we move on to the effects of the quadrupolar variation in solute concentration. While the uniform gradient case featured results found by Anderson *et al.* (1982) (and verified here), the analysis of the non-uniform gradient is entirely novel to the present study. Using the same asymptotic matching strategy as before, we find the following solution for the disturbed quadrupolar solute field:

$$Q=\begin{cases}Q^{O}(\rho)=\rho^2+\dfrac{2}{3}\rho^{-3}\left(1-5\dfrac{K}{L}\lambda+O(\lambda^2)\right) & \text{for } \rho-1\gg\lambda,\\ Q^{I}(y)=\dfrac{5}{3}\left(1-2\dfrac{K}{L}\lambda+O(\lambda^2)\right)\exp\left(-\phi^{*}(y)\right) & \text{for } \rho-1\lesssim\lambda.\end{cases} \tag{4.25}$$

The quadrupolar solute field yields the following exact expressions for the stream functions:

$$\psi_{\beta}(\rho)=\frac{1}{2}\left(\xi'_{\beta}(1)-\frac{\xi''_{\beta}(1)+3\,\xi'_{\beta}(1)}{5(1+\sigma)}\right)\left(\frac{1}{\rho^2}-1\right)+\xi_{\beta}(\rho)-\xi_{\beta}(1), \tag{4.26a}$$

$$\tilde{\psi}_{\beta}(\rho)=\frac{\xi''_{\beta}(1)+3\,\xi'_{\beta}(1)}{10(1+\sigma)}(\rho^5-\rho^3), \tag{4.26b}$$

where ξ_{β}, the particular solution of (3.10*a*,*b*), is given by

$$\xi_{\beta}(\rho)=\frac{1}{10}\int_{\rho}^{\infty}\left[\frac{3}{7}\left(\frac{v^5}{\rho^2}-\frac{\rho^5}{v^2}\right)+\rho^3-v^3\right]Q(v)\,\frac{\mathrm{d}\phi^{*}}{\mathrm{d}v}\,\mathrm{d}v. \tag{4.27}$$

Again, in the inner region of (4.25), the concentration profile can be expressed as the product of the Boltzmann factor with the outer-region solution, $Q^{O}(\rho)$, evaluated approaching the inner region, that is,

$$Q^{I}(y)=Q^{O}(1)\exp\left(-\phi^{*}(y)\right), \tag{4.28}$$

where $Q^{O}(1)$ is the outer-region solution evaluated at $\rho=1$. Applying (4.28) to (4.27) and performing integration by parts, we obtain

$$\xi_{\beta}(\rho)=\frac{Q^{O}(1)}{10}\int_{\rho}^{\infty}\left[\frac{3}{7}\left(5\frac{v^4}{\rho^2}+2\frac{\rho^5}{v^3}\right)-3v^2\right][\exp\left(-\phi^{*}(v)\right)-1]\mathrm{d}v. \tag{4.29}$$

Switching to the inner coordinate y and expanding for small values of λ, we obtain

$$\xi_{\beta}(y)=5\lambda^3\left(1-2\lambda\frac{K}{L}\right)\int_{y}^{\infty}\frac{(y-x)^2}{2}[\exp\left(-\phi^{*}(x)\right)-1]\mathrm{d}x+O(\lambda^5). \tag{4.30}$$

https://doi.org/10.1017/jfm.2022.666 Published online by Cambridge University Press

These solutions can be used to compute the hydrodynamic stress jump due to the quadrupolar solute field at the surface of a spherical drop, which is found to equal

$$\Pi_{rr}^{\beta *} - \tilde{\Pi}_{rr}^{\beta *} = \left[\frac{1}{3}(\psi_\beta''' - \sigma\tilde{\psi}_\beta''') - 6(\psi_\beta' - \sigma\tilde{\psi}_\beta') + 12(\psi_\beta - \sigma\tilde{\psi}_\beta)\right]_{\rho=1}. \tag{4.31}$$

Inserting the stream function solution (4.26) into (4.31) gives

$$\Pi_{rr}^{\beta *} - \tilde{\Pi}_{rr}^{\beta *} = \left(\frac{1}{3}\xi_\beta''' - \frac{2+3\sigma}{5(1+\sigma)}\xi_\beta'' - \frac{26+29\sigma}{5(1+\sigma)}\xi_\beta'\right)\Bigg|_{\rho=1}. \tag{4.32}$$

Converting (4.32) into terms of the inner coordinate and applying (4.30) yields

$$\Pi_{rr}^{\beta *} - \tilde{\Pi}_{rr}^{\beta *} = -Q^O(1)\left\{[\exp(-\phi^*(R)) - 1] + \frac{3(2+3\sigma)}{5(1+\sigma)}\lambda\frac{K}{L} + O(\lambda^2)\right\}. \tag{4.33}$$

This time, the viscosity ratio appears in the stress jump, in contrast to (4.14). Solving for the solute-interactive stress for the quadrupolar case is obtained by a calculation equivalent to (4.3), which yields

$$\Sigma^{\beta *} = Q^O(1)\left\{[\exp(-\phi^*(R)) - 1] + 2\lambda\frac{K}{L} + 2\lambda^2\frac{K}{L}\frac{I}{L}\right\}. \tag{4.34}$$

Finally, from (3.15), these stresses are found to cause a deformation characterized by the magnitude

$$\delta_\beta = \frac{1}{6}\left(\Pi_{rr}^{\beta *} - \tilde{\Pi}_{rr}^{\beta *} + \Sigma^{\beta *}\right) = \frac{4+\sigma}{18(1+\sigma)}\lambda\frac{K}{L} + O(\lambda^2). \tag{4.35}$$

The deformed shape of the drop is therefore given by the equation

$$r_d(\theta) = R\left(1 + \frac{4+\sigma}{18(1+\sigma)}\frac{\beta k_B T R^2 K}{\gamma}\frac{3\cos^2\theta - 1}{2}\right), \tag{4.36}$$

where r_d is an angularly dependent distance from the drop centroid that describes the deformed surface. The appropriate capillary number is $\beta k_B T R^2 K/\gamma$, rather than $\beta k_B T R^3/\gamma$ as our evidently naive scaling analysis had suggested. Indeed, the capillary number should have a dependence on the drop–solute interaction strength, as K provides. The adsorption length K is often, but not always, smaller than the drop radius R (Anderson & Prieve 1990). The deformed shape predicted in (4.36) is spheroidal. Whether this spheroid is oblate or prolate depends on the sign of the adsorption length ($K > 0$ for an attractive interaction). The drop is made prolate when K is positive, and oblate when K is negative. These behaviours are illustrated in figure 2.

For a drop in a background flow field, the capillary number characterizing deformation is $Ca_f = \eta\dot{\epsilon}R/\gamma$, where $\dot{\epsilon}$ is the shear rate of the flow. For diffusiophoresis, we have shown that the relevant capillary number is $Ca = \beta R^2 K k_B T/\gamma$; the ratio is $Ca/Ca_f = \beta R K k_B T/\dot{\epsilon}\eta$. Thus we expect deformation due to diffusiophoresis to be more prominent for larger drops. Now, consider a uniaxial extensional flow whose axis of extension is along the direction (z) of drop translation due to diffusiophoresis. This flow would elongate the drop into a prolate shape. Thus diffusiophoresis would aid this deformation for $K > 0$, and suppress deformation for $K < 0$. It may appear surprising that the deformation does not vanish in the limit of a rigid particle, $\sigma \to \infty$. However, recall that we assumed that a

https://doi.org/10.1017/jfm.2022.666 Published online by Cambridge University Press

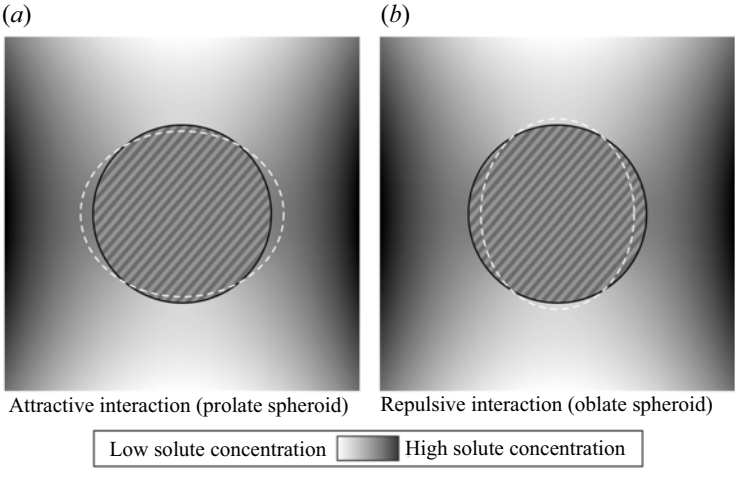


Figure 2. Deformation of a fluid drop undergoing diffusiophoresis in a quadrupolar solute distribution. The undeformed spherical shape is represented by the cross-hatched circle, while the deformed spheroidal shape is represented by a superimposed dashed white ellipse. The shapes are rotationally symmetric around the horizontal centre axis. The surrounding quadrupolar solute concentration from the outer region of (4.25) is represented by shading. (*a*) For an attractive interaction, the drop protrudes into areas of high ambient concentration, and flattens in areas of low concentration. (*b*) For a repulsive interaction, this trend is reversed.

steady state has been achieved. While a non-zero deformation is found for $\sigma \to \infty$ under this assumption, we anticipate the relaxation time scale for an initially spherical drop to reach this steady state becomes infinitely long in this limit. A similar situation occurs for drop deformation under an extensional flow field (Leal 2007), meaning that as $\sigma \to \infty$, the drop would take an infinite amount of time to reach the predicted steady-state deformation shape.

5. Concluding discussion

In this work, we have analysed the deformation of a fluid drop undergoing diffusiophoresis in a non-uniform gradient of neutral solute. We have made a number of simplifying (yet physically reasonable) assumptions to enable analytical progress, namely (i) zero solute Péclet number, (ii) zero fluid Reynolds number, (iii) small capillary number, and (iv) the thin-interfacial-layer limit. Relaxing these assumptions would lead to a nonlinear coupling between the deformation observed in a quadratic field and the translation speed driven by the uniform component of the solute gradient. We have also stipulated that solute does not reside within the drop. If this assumption were to be relaxed, then we expect the result of zero deformation under a uniform gradient to persist, but the deformation of the drop under a non-uniform gradient would be affected by solute interactions within the drop. We find in (4.18) that a drop in a uniform gradient has no tendency to deform at zero Reynolds number. In the case of small capillary number $Ca = \beta k_B T R^2 K/\gamma$, we find that a non-uniform gradient induces a spheroidal deformation of the form (4.36). Thus (4.18) and (4.36) represent the two main mathematical results of our analysis. Our work therefore suggests that drop deformation during diffusiophoresis is possible, in principle. We now consider the practicality of observing this effect.

One way to estimate the possible magnitudes of the quadrupolar variation β is to consider solute diffusion into a pore, a case which is of experimental interest (Kar *et al.* 2015; Shin *et al.* 2016). For a sufficiently long one-dimensional pore initially void of solute,

https://doi.org/10.1017/jfm.2022.666 Published online by Cambridge University Press

which is then exposed to a solute concentration C_0 at its mouth ($z = 0$), the solute profile in time and space is governed by

$$C(z, t) = C_0 \operatorname{erfc}\left(\frac{z}{2\sqrt{Dt}}\right), \tag{5.1}$$

where erfc is the complementary error function. The magnitude of the quadratic gradient in one dimension is the second spatial derivative of this profile, $\beta = \partial^2 C/\partial z^2$. This can be used to estimate a capillary number in different regions of time and space in the pore, which would in turn determine the extent of drop deformation via (4.36). Consider an oil droplet ($R = 10\ \mu\text{m}$, $\gamma = 40\ \text{mN m}^{-1}$) in an aqueous gradient of solute ($D = 600\ \mu\text{m}^2\ \text{s}^{-1}$) at room temperature ($T = 298$ K). Let the imposed solute concentration outside the pore be $C_0 = 1$ M. Due to the large range of evolving ambient concentrations experienced by a drop immersed in the pore, we include variation of the adsorption length K due to ambient concentration, following a Langmuir adsorption isotherm (Anderson *et al.* 1982), such that

$$K = \frac{K_0}{1 + K_0 C/\Gamma_{sat}}, \tag{5.2}$$

where K_0 is the initial adsorption length at low solute concentrations, and Γ_{sat} is the saturated surface concentration of the solute. The latter can be estimated by the cross-section of molecular close packing $\Gamma_{sat} = 1/(30\ \text{Å}^2)$, and the initial adsorption length is estimated at $K_0 = 5\ \mu\text{m}$. The effect of incorporating (5.2) is that the capillary number is unaffected at low solute concentrations but dampened at higher concentrations due to saturation effects. With these parameters established, we can then plot the capillary number on a logarithmic scale, which is shown in figure 3. We find that in this situation, a capillary number of 0.1, for which our theory is applicable, is attainable for about 6 s over a region of 200 μm, and is marked by a dashed line in figure 3. Note that $O(1)$ values of Ca could be attained very near the mouth of the pore at short times, but our theory is not applicable here. Therefore, the possibility of sustaining deformation in a way that could significantly affect diffusiophoretic transport, via the fluid–structure coupling suggested in § 1, seems unlikely in this scenario. This is a possible explanation for why deformation has not been reported in experiments involving diffusiophoresis of oil drops (Yang *et al.* 2018). Note that the magnitude of the deformation is predicted to increase with the value of the capillary number $Ca = \beta R^2 K k_B T/\gamma$. Thus for a fixed non-uniformity in the gradient (β), an increased deformation would be achieved by increasing the drop size (R), adsorption length (K) or temperature (T), or by lowering the interfacial tension (γ).

We have considered the simplest case of a deformable object: a Newtonian fluid drop. It would be interesting to consider other types of deformable objects, e.g. an elastic capsule, vesicle, etc. undergoing neutral-solute diffusophoresis. A particular question here is whether there would remain no tendency for deformation in a uniform gradient, or is the drop a special result? In this regard, it may be important to consider the role of hydrodynamic slip at the interface of such objects. This could be done by including a Navier-slip condition at the interface of the object, and suspending fluid to relax (2.5), as was done in the context of the shear rheology of emulsions by Ramachandran & Leal (2012).

It would also be valuable to extend the ideas in this work to examine the local stress distribution, and thus the possibility of drop deformation, during electrophoretic motion in an ionic solution. Of course, the problem of electrophoresis of a drop has been considered previously (Baygents & Saville 1991), but those studies have assumed that

https://doi.org/10.1017/jfm.2022.666 Published online by Cambridge University Press

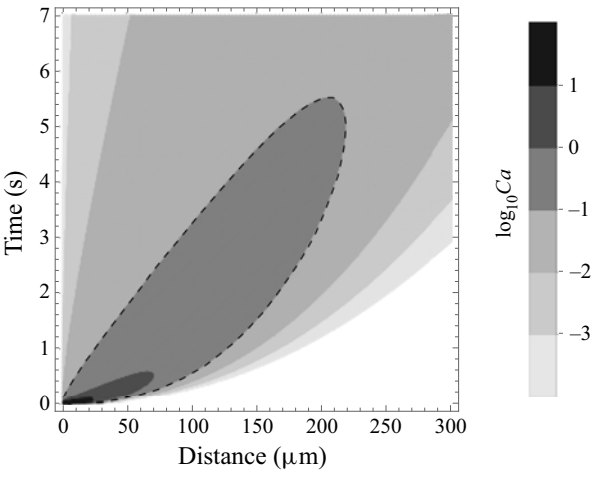


Figure 3. Temporal and spatial variation of capillary number in a one-dimensional pore. This contour plot shows the base-10 logarithm of the capillary number $Ca = \beta k_B T R^2 K/\gamma$, which gives the order of magnitude of the deformation normalized by the drop radius, as a function of time and space in a pore initially void of solute. Parameter values are explained in the main text. The curve on which $Ca = 0.1$ is marked by a dashed line.

the drop remains spherical. For a rigid particle undergoing electrophoresis in a uniform electrolyte concentration, Marbach *et al.* (2020) predicted no local stress and hence no deformation due to cancellation of hydrodynamic and electric (Maxwell) forces. However, our analysis suggests the need to consider the internal stresses for a fluid drop. The electrophoresis problem would also be relevant to a drop undergoing diffusiophoresis in an electrolyte with unequal cationic and anionic diffusion coefficients, since in such cases a spontaneous electric field develops that drives electrophoretic motion, in addition to 'chemiphoretic' motion due to the imposed concentration gradient. The following differences occur for electrolyte diffusiophoresis as compared to neutral solutes: (i) there are now two charged solute species (cations and anions) coupled to the local electric field via a Poisson equation; (ii) the solute interactive body force $-C\nabla\phi$ in the momentum balance is replaced by the Coulomb body force, i.e. the product of the local charge density and electric field; and (iii) the tangential stress balance is not solely hydrodynamic and now includes Maxwell stresses.

Funding. This work was funded by Procter and Gamble. H.C.W.C. also acknowledges the startup funding support from the Division of Sponsored Programs, Department of Chemical Engineering, and Herbert Wertheim College of Engineering at University of Florida.

Declaration of interests. The authors report no conflict of interest.

Author ORCIDs.
Brian E. McKenzie https://orcid.org/0000-0003-4477-8845;
Henry C.W. Chu https://orcid.org/0000-0002-2705-0863;
Aditya S. Khair https://orcid.org/0000-0001-6076-2910.

References

Abécassis, B., Cottin-Bizonne, C., Ybert, C., Ajdari, A. & Bocquet, L. 2009 Osmotic manipulation of particles for microfluidic applications. *New J. Phys.* **11** (7), 785–789.
Anderson, J.L. 1989 Colloid transport by interfacial forces. *Annu. Rev. Fluid Mech.* **21**, 61–99.

https://doi.org/10.1017/jfm.2022.666 Published online by Cambridge University Press

ANDERSON, J.L., LOWELL, M.E. & PRIEVE, D.C. 1982 Motion of a particle generated by chemical gradients. Part 1. Non-electrolytes. *J. Fluid Mech.* **117**, 107–121.

ANDERSON, J.L. & PRIEVE, D.C. 1990 Diffusiophoresis caused by gradients of strongly adsorbing solutes. *Langmuir* **7**, 403–406.

AULT, J.T., WARREN, P.B., SHIN, S. & STONE, H.A. 2017 Diffusiophoresis in one-dimensional solute gradients. *Soft Matt.* **13**, 9015–9023.

BANERJEE, A., WILLIAMS, I., NERY-AZEVEDO, R., HELGESON, M.E. & SQUIRES, T.M. 2016 Soluto-inertial phenomena: designing long-range, long-lasting, surface-specific interactions in suspensions. *Proc. Natl Acad. Sci. USA* **113** (31), 8612–8617.

BAYGENTS, J.C. & SAVILLE, D.A. 1988 The migration of charged drops and bubbles in electrolyte gradients: diffusiophoresis. *Physico-Chem. Hydrodyn.* **10**, 543–560.

BAYGENTS, J.C. & SAVILLE, D.A. 1991 Electrophoresis of drops and bubbles. *J. Chem. Soc. Faraday Trans.* **87**, 1883–1898.

DECAYEUX, J., DAHIREL, V., JARDAT, M. & ILLIEN, P. 2021 Spontaneous propulsion of an isotropic colloid in a phase-separating environment. *Phys. Rev.* E **104**, 034602.

DERJAGUIN, B.V., SIDORENKOV, G.P., ZUBASHCHENKOV, E.A. & KISELEVA, E.V. 1947 Kinetic phenomena in boundary films of liquids. *Kolloidn. Z.* **9**, 335–347.

KAR, A., CHIANG, T.Y., ORTIZ RIVERA, I., SEN, A. & VELEGOL, D. 2015 Enhanced transport into and out of dead-end pores. *ACS Nano* **9**, 746–753.

KEH, H.J. & WANG, J.C. 2001 Diffusiophoresis of colloidal spheres in nonelectrolyte gradients at small but finite Péclet numbers. *Colloid Polym. Sci.* **279**, 305–311.

KHAIR, A.S. 2013 Diffusiophoresis of colloidal particles in neutral solute gradients at finite Péclet number. *J. Fluid Mech.* **731**, 64–94.

LEAL, L.G. 2007 *Advanced Transport Phenomena: Fluid Mechanics and Convective Transport Processes*. Cambridge University Press.

MARBACH, S., YOSHIDA, H. & BOCQUET, L. 2020 Local and global force balance for diffusiophoretic transport. *J. Fluid Mech.* **892**, A6.

MICHELIN, S. & LAUGA, E. 2014 Phoretic self-propulsion at finite Péclet numbers. *J. Fluid Mech.* **747**, 572–604.

MORAN, J.L. & POSNER, J.D. 2017 Phoretic self-propulsion. *Annu. Rev. Fluid Mech.* **49** (1), 511–540.

MORRISON, F.A. 1970 Electrophoresis of a particle of arbitrary shape. *J. Colloid Interface Sci.* **34**, 210–214.

NERY-AZEVEDO, R., BANERJEE, A. & SQUIRES, T.M. 2017 Diffusiophoresis in ionic surfactant gradients. *Langmuir* **33**, 9694–9702.

PALACCI, J., COTTIN-BIZONNE, C., YBERT, C. & BOCQUET, L. 2012 Osmotic traps for colloids and macromolecules based on logarithmic sensing in salt taxis. *Soft Matt.* **8**, 980–994.

PAXTON, W.F., KISTLER, K.C., OLMEDA, C.C., SEN, A., ST. ANGELO, S.K., CAO, Y., MALLOUK, T.E., LAMMERT, P.E. & CRESPI, V.H. 2004 Catalytic nanomotors: autonomous movement of striped nanorods. *J. Am. Chem. Soc.* **126**, 13424–13431.

PRIEVE, D.C., EBEL, J.P. & LOWELL, M.E. 1984 Motion of a particle generated by chemical gradients. Part 2. Electrolytes. *J. Fluid Mech.* **148**, 247–269.

RAMACHANDRAN, A. & LEAL, L.G. 2012 The effect of interfacial slip on the rheology of a dilute emulsion of drops for small capillary numbers. *J. Rheol.* **56** (6), 1555–1587.

RAMM, B., GOYCHUK, A., KHMELINSKAIA, A., BLUMHARDT, P., ETO, H., GANZINGER, K.A., FREY, E. & SCHWILLE, P. 2021 A diffusiophoretic mechanism for ATP-driven transport without motor proteins. *Nat. Phys.* **17**, 850–858.

RUCKENSTEIN, E. 1981 Can phoretic motions be treated as interfacial tension gradient driven phenomena? *J. Colloid Interface Sci.* **83**, 77–81.

SEAR, R.P. 2019 Diffusiophoresis in cells: a general nonequilibrium, nonmotor mechanism for the metabolism-dependent transport of particles in cells. *Phys. Rev. Lett.* **122**, 128101.

SHIN, S. 2020 Diffusiophoretic separation of colloids in microfluidic flows. *Phys. Fluids* **32** (10), 101302.

SHIN, S., UM, E., SABASS, B., AULT, J.T., RAHIMI, M., WARREN, P.B. & STONE, H.A. 2016 Size-dependent control of colloid transport via solute gradients in dead-end channels. *Proc. Natl Acad. Sci. USA* **113**, 257–261.

SHIN, S., WARREN, P.B. & STONE, H.A. 2018 Cleaning by surfactant gradients: particulate removal from porous materials and the significance of rinsing in laundry detergency. *Phys. Rev. Appl.* **9**, 034012.

TAYLOR, T.D. & ACRIVOS, A. 1964 On the deformation and drag of a falling viscous drop at low Reynolds number. *J. Fluid Mech.* **18**, 466–476.

VELEGOL, D., GARG, A., GUHA, R., KAR, A. & KUMAR, M. 2016 Origins of concentration gradients for diffusiophoresis. *Soft Matt.* **12**, 4686–4703.

https://doi.org/10.1017/jfm.2022.666 Published online by Cambridge University Press

WARREN, P.B. 2020 Non-Faradaic electric currents in the Nernst–Planck equations and nonlocal diffusiophoresis of suspended colloids in crossed salt gradients. *Phys. Rev. Lett.* **124**, 248004.
YANG, F., SHIN, S. & STONE, H.A. 2018 Diffusiophoresis of a charged drop. *J. Fluid Mech.* **852**, 37–59.
YOUNG, N.O., GOLDSTEIN, J.S. & BLOCK, M.J. 1959 The motion of bubbles in a vertical temperature gradient. *J. Fluid Mech.* **6**, 350–356.

https://doi.org/10.1017/jfm.2022.666 Published online by Cambridge University Press